Topics in Catalysis 2 (1995) 17–27

Synthesis and catalytic properties of eggshell cobalt catalysts for the Fischer–Tropsch synthesis

Enrique Iglesia

Department of Chemical Engineering, University of California at Berkeley, Berkeley, CA 94720, USA

Stuart L. Soled, Joseph E. Baumgartner and Sebastian C. Reyes

Corporate Research Laboratories, Exxon Research and Engineering Co., Route 22 East, Annandale, NJ 08801, USA

CO diffusional restrictions decrease C_{5+} synthesis rates and selectivity within large (1–3 mm) catalyst pellets often required in Fischer–Tropsch (FT) synthesis reactors. Eggshell catalysts, where Co is located preferentially near outer pellet surfaces, reduce the severity of these transport restrictions and lead to higher synthesis rates and C_{5+} selectivity. Maximum C_{5+} selectivities occur on catalysts with intermediate shell thickness, within which transport restrictions limit the removal of reactive olefins but not the arrival of reactants at catalytic sites. A new synthetic technique leads to sharp distributions of active sites near outer pellet surfaces by controlling the rate of imbibition of cobalt nitrate melts. Also, slow reduction of the impregnated salt leads to moderate Co dispersions (0.05–0.10) even at high local Co loadings present within shell regions.

Keywords: Fischer–Tropsch synthesis; cobalt catalysts; eggshell catalysts; diffusional restrictions; CO hydrogenation

1. Introduction

FT synthesis within packed-bed reactors requires large pellets (1–3 mm diameter) in order to ensure acceptable pressure gradients across the catalyst bed; it also requires very active catalysts to minimize reactor volumes required to reach desired conversion levels. Previously, we showed that FT synthesis turnover rates on Co and Ru catalysts depend weakly on metal dispersion and on metal oxide support (e.g., TiO_2, SiO_2, Al_2O_3, etc.) [1], but that reaction selectivity is influenced strongly by a complex coupling among diffusion, reaction, and convection processes within catalyst pellets and reactors [1–5]. Here, we report the synthesis of uniform and eggshell Co distributions within SiO_2 pellets, which exploit this coupling to lead to maximum C_{5+} selectivities at intermediate severities of transport restrictions. The benefits of non-uniform intrapellet site distributions have been previously reported for many catalytic reactions [6–12].

2. Experimental

Co/SiO_2 powders (0.143 mm average pellet diameter) were uniformly impregnated by contacting an acetone/SiO_2 slurry (Davison 62, W.R. Grace Co., 280 $m^2 g^{-1}$) with a solution of Co nitrate (Alfa) in acetone. Large Co/SiO_2 pellets were also uniformly impregnated by incipient wetness impregnation of silica spheres (Shell S980G: 115 $m^2 g^{-1}$, 2.2 mm diameter; Shell S980B; 1.7 mm diameter; 260 $m^2 g^{-1}$) with an aqueous solution of Co nitrate. This sample was then crushed and sieved to form pellets with diameters between 0.125 and 1.7 mm.

Capillary imbibition rates were measured by attaching individual SiO_2 spheres (Shell S980B) to a wooden stick using epoxy resin and submerging the spheres in nitrate solutions and melts for controlled periods of time. More viscous solutions (solution B) were prepared by adding 1.0 wt% hydroxyethylcellulose (HEC) to solution A to increase its viscosity to the same value as the melt. Another solution with much lower Co nitrate concentration (0.01 g/cm^3) was prepared to study the imbibition of very dilute solutions (solution C). Melts at 333 and 348 K were used to explore the effect of temperature and of local melt solidification during impregnation. Solution viscosities and surface tensions were measured with a Nametre vibrating sphere viscometer and a Kruss K-10 ring tensiometer, respectively.

Silica spheres were immersed in selected solutions and melts for 2–48 s. These immersion experiments were repeated using heated (383 K) and cooled (263 K) spheres. In each case, 10–20 spheres were individually immersed for the specified time, any excess liquid was removed, and the spheres were dried in air at room temperature for 0.5 h. These samples were then calcined in air at 623 K for 0.25 h to form Co_3O_4, a compound that provided sharp visual contrast in measurements of eggshell thickness using optical microscopy.

Eggshell catalysts were also prepared by placing SiO_2 spheres (Shell S980G, 12.5 g) into a funnel (5.5 cm diameter) containing a 15–20 mm layer of 6 mm nonporous glass beads next to its fritted bottom. Molten Co nitrate at 348–363 K (50 g, melting point $\sim$ 323 K) was poured uniformly over the spheres (2–3 cm bed height). The spheres were stirred with a glass rod, and vacuum was used to rapidly remove the molten nitrate salt and to limit contact times to 2–4 s. Samples were also prepared using this technique and aqueous solutions of Co nitrate (solution A, table 2) at room temperature instead of the nitrate melt. After drying at 373 K, all catalysts were reduced in flowing hydrogen by increasing the temperature from 373 to 693–723 K at 6–12 K h^{-1} and holding at 693–723 K for 4–16 h. They were passivated by contact with a dilute oxygen stream (1% O_2/He) at room temperature and then re-reduced at 693–723 K for 2–4 h before catalytic and chemisorption measurements.

All catalysts were characterized by X-ray diffraction, H_2 chemisorption, N_2 physisorption, and optical microscopy. Cobalt dispersions were calculated from hydrogen chemisorption uptakes at 373 K, assuming a 1 : 1 H : Co surface stoichiometry. FT synthesis rates and selectivities were measured in an isothermal

(±1 K) plug-flow reactor at 473 K and 2000 kPa, using stoichiometric feeds ($H_2/CO = 2.0$–2.1). Passivated catalysts were re-reduced in flowing H_2 at 623 K, cooled to 473 K, and exposed to reactants. All reported data were obtained after 24–48 h on stream. Synthesis products were analyzed by gas and gel-permeation chromatography [1]. Reaction rates are reported as metal–time yields (molar CO conversion rates per g-atom Co) and site–time yields (molar CO conversion rate per g-atom surface Co). Selectivities are reported as the percentage of reacted CO appearing as each product.

3. Results and discussion

At typical FT synthesis conditions, two types of coupled reaction–diffusion processes occur with catalyst pellets: diffusion-limited product removal and reactant arrival. In the first type, the extent of α-olefin readsorption and the molecular weight and paraffin content of products increase as bed residence time, pellet size, or active site density increase. In the second type, catalyst pellets become depleted of CO and favor the formation of lighter products. The opposing effects of these two types of transport restrictions lead to maximum C_{5+} selectivities when porous structures introduce transport restrictions of intermediate severity [3,4].

3.1. PELLET DIAMETER EFFECTS ON FT SYNTHESIS RATE AND SELECTIVITY

Pellet diameter effects on synthesis rate and selectivity were determined by measuring FT synthesis rates and selectivities on Co sites uniformly distributed within SiO_2 pellets of 0.13, 0.165, 0.36, 0.86, and 1.5 mm diameter (24.8% wt. Co) (table 1). These catalysts were prepared by crushing and sieving a single batch of uniformly impregnated SiO_2 spheres (1.7 mm diameter, 260 $m^2\,g^{-1}$).

Table 1
Pellet diameter effects on Fischer–Tropsch synthesis rate and selectivity

pellet diameter (mm)	0.13	0.165	0.36	0.86	1.7
characteristic diffusion distance (mm)	0.065	0.0825	0.18	0.425	0.75
structural parameter [a] $\chi(m^{-1}) \times 10^{-16}$	70	122	536	2988	9800
Co–time yield (h^{-1})	4.30	3.99	4.09	3.98	3.61
site–time yield (h^{-1})	110	102	105	102	93
CH_4 selectivity (%)	8.1	6.6	5.9	8.7	12.2
C_{5+} selectivity (%)	81.0	82.3	87.1	82.0	80.8
CO_2 selectivity (%)	0.20	0.22	0.45	0.80	1.2
(1-hexene/*n*-hexane) ratio	1.25	1.10	1.03	0.20	0.06

[a] $\chi = L^2\phi\theta/r_p$; r_p pore radius in m, site density (θ) in Co atoms/m^2, L as twice the characteristic diffusion distance in m. Conditions: 474 K, 2000 kPa, $H_2/CO = 2.08$, 60–65% CO conversion, starting material 24.8% Co/SiO_2, 1.7 mm pellet diameter, 260 $m^2\,g^{-1}$, 3.9% Co dispersion, site density $= 0.51 \times 10^{-6}$ g-atom surface Co/m^2.

Methane and CO_2 selectivities increase and C_{5+} selectivity decreases as pellet diameter increases above 0.36 mm. Methane selectivity increases because transport restrictions decrease CO concentrations within larger pellets. At low CO concentrations, FT synthesis kinetics favor light paraffins, the predominant products on severely transport-limited pellets. C_{5+} selectivity and the olefin content decrease with increasing pellet size. Higher CO_2 selectivities on large pellets apparently reflect transport-limited water–gas shift reactions, enhanced by slow removal of water. CO_2 selectivity increases with increasing CO conversion and water concentration, suggesting that CO_2 forms predominantly via secondary water–gas shift reactions. A similar increase in water concentration occurs within larger pellets as they become increasingly unable to remove the water product of FT synthesis steps; this leads to faster water–gas shift reactions and to higher CO_2 selectivities. Water removal and CO arrival become limited by transport rates in the same pellet diameter range.

FT synthesis rates, however, are not influenced strongly by pellet diameter, in the range where selectivity is strongly affected (0.36–1.7 mm). This reflects the negative order of FT synthesis kinetics in the diffusion-limited reactant (CO) [4]. This type of kinetics delays the decrease in catalyst productivity that ultimately occurs as reactant transport limitations become increasingly severe for pellet diameters larger than 1.7 mm. On small pellets, C_{5+} selectivity actually increases with increasing pellet diameter because transport restrictions slow down the removal of α-olefins and enhance their readsorption and chain initiation reactions. Maximum C_{5+} selectivities are obtained on pellets of intermediate diameter, where olefin removal is slow but reactants remain unrestricted by transport limitations.

3.2. SYNTHESIS AND CHARACTERIZATION OF EGGSHELL CATALYST PELLETS

The effects of viscosity, surface tension, and pore structure on liquid penetration rates were determined by immersing individually mounted silica spheres (2.7 mm diameter) into nitrate melts or solutions (table 2, fig. 2). Hydroxyethyl-

Table 2
Properties of impregnating nitrate solutions and melts

Impregnating liquid	Hydroxy ethylcellulose (wt%)	Viscosity μ (cp)	Surface tension γ (dynes cm^{-1})
solution A [a]	0	3.2 (298 K)	65.6
solution B [a]	1.0	45 (298 K)	66.4
melt	0	48 (333 K)	–
melt	0	31 (348 K)	66.2
solution C [b]	0	0.93 (298 K)	66.9
water	0	0.92 (295 K)	70.6

[a] 0.5 g Co nitrate/cm^3 H_2O.
[b] 0.01 g Co nitrate/cm^3 H_2O.

cellulose (HEC) was added to some solutions in order to increase their viscosity to the values of nitrate melts. For example, the bulk viscosity of solution B (0.5 g Co nitrate/cm^3 H_2O, 1% wt. HEC) at room temperature (RT) was 45 cp, similar to that of nitrate melts (48 cp at 333 K).

The surface tension of nitrate solutions was not influenced strongly by temperature or by adding HEC and is similar to those of nitrate melts (table 2). The penetration rate of nitrate melts (at 333 K) into silica spheres (2.7 mm diameter, 210 $m^2 g^{-1}$) is much slower than that of nitrate solutions of similar viscosity and surface tension at RT (curves C and B, fig. 2). Both melts and viscosified solutions, however, penetrate silica spheres less rapidly than aqueous nitrate solutions without HEC (fig. 1 and curve A in fig. 2). Melt imbibition rates into silica spheres heated (383 K; C″) or cooled (263 K; C′) before immersion resemble those on spheres held at RT, because thermal equilibration between the spheres and the melt occurs very rapidly upon immersion (fig. 2).

Melts form eggshells with thickness less than 0.20 mm, even at 30 s contact times (figs. 1 and 2). Longer contact times increase shell thickness and ultimately lead to complete penetration. In fig. 2, liquid penetration depths are plotted against $t^{1/2}$, as suggested by Washburn [17]. The position of the liquid front is controlled by liquid and solid properties, such as liquid viscosity (μ) and surface tension (γ), support pore radius (r_0), pore structure tortuosity (τ), and contact angles between the liquid and the support surface (θ). The dimensionless penetration depth ($\zeta = r/r_0$) of weakly adsorbing solutions forming thin shells within spherical pellets is described by

$$\zeta = \Omega t^{1/2}, \tag{1}$$

where

$$\Omega = [(1/\tau R_0^2)\gamma_0 r_p \cos(\theta)/2\mu]^{1/2}. \tag{2}$$

These equations apply rigorously only to cylindrical capillaries. As an approxima-

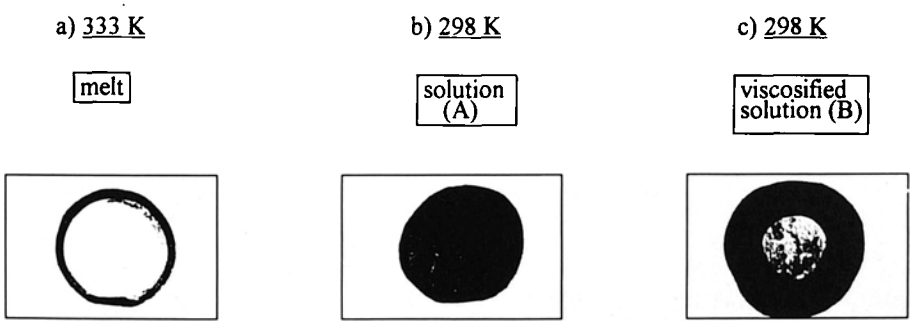

Fig. 1. Optical micrograph of impregnated silica pellets (vacuum filtration procedures, 32 s contact time).

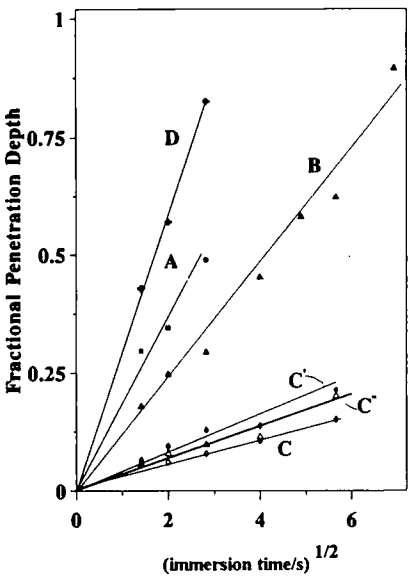

Fig. 2. Effect of impregnating solution on liquid penetration depth (SiO_2: 210 m^2/g; 2.7 mm diameter. (A) Solution A; 0.5 g Co nitrate/cm^3 H_2O; (B) solution B; 0.5 g Co nitrate/cm^3 H_2O plus 1% HEC; (C) nitrate melt, SiO_2 at 298 K; (C′) nitrate melt, SiO_2 at 373 K; (C″) nitrate melt, SiO_2 at 383 K; (D) solution C; 0.01 g Co nitrate/cm^3 H_2O.

tion, they also describe the process within more complex porous structures at small penetration depths. Eq. (1) suggests that a plot of ζ versus $t^{1/2}$ is a straight line of slope Ω. Estimates of Ω require accurate measurements of γ_0, r_p, θ, and μ. Then, eqs. (1) and (2) provide an adequate description of the fluid motion within our porous supports (table 3).

The slopes of the linear region in such curves and those calculated from eq. (2)

Table 3
Liquid penetration rates. Comparison of experimental values and model predictions

Impregnating liquid/solution	Liquid temperature (K)	Sphere diameter $2R_0$ (cm)	Average pore radius r_p (nm)	Slope (from fig. 2) ($s^{-1/2}$)	Slope (from eq. (2)) ($s^{-1/2}$)
A	298	0.27	8.5	0.18	0.16
B	298	0.27	8.5	0.12	0.045
B	298	0.22	16.0	0.12	0.075
melt	333	0.27	8.5	0.028	0.042
melt	333	0.22	16.0	0.085	0.074
melt (silica at 383 K)	348	0.27	8.5	0.035	0.052
melt (silica at 263 k)	348	0.27	8.5	0.041	0.052
C	298	0.27	8.5	0.29	0.31

using measured pore structure and solution properties (for $\theta = 0$, $\tau = 1.8$), agree well for nitrate melts and solutions and differ significantly only for viscosified nitrate solutions (table 3), which penetrate significantly faster than predicted by the imbibition model. Pellets impregnated with solution B (1% HEC) and heated to 673 K in N_2 for 8–16 h show that much of the HEC additive remains on the external pellet surfaces during imbibition. Therefore, the viscosity of the solution within pores is much lower than in the bulk liquid.

We have exploited the slow penetration of nitrate melts into SiO_2 by preparing larger quantities of eggshell pellets (10–20 g) using the vacuum filtration techniques described in section 2. Larger amounts were also prepared by contacting spheres contained within a rotating cylinder with nitrate melts at controlled temperature conditions.

Vacuum filtration using nitrate melts produces pellets with Co (10–13% wt.) located exclusively within 0.1–0.2 mm eggshells near outer pellet surfaces (fig. 1a, 5 s contact time). The local Co concentration within the eggshell region is 30–40% wt. Similar vacuum filtration techniques using aqueous Co nitrate solutions (solution A, table 2) led to complete penetration into the SiO_2 spheres, even at contact times shorter than 5 s (fig. 1b). When the solution viscosity was increased to the same level as the melts by HEC addition, penetration was slower but still significantly faster than that of the melt (fig. 1c).

3.3. FT SYNTHESIS RATE AND SELECTIVITY ON EGGSHELL AND UNIFORM PELLETS

We have measured FT synthesis rates and detailed product distributions on even and eggshell pellets (2.2 mm, diameter) both as intact pellets and as powders formed by grinding these pellets to an average diameter of 0.143 mm (table 4). We have also compared ground pellets with directly impregnated silica powders.

The range of cobalt dispersion (0.050–0.063) in eggshell catalysts is similar to those in even pellets or powders, in spite of the much higher Co concentrations within shell regions in eggshell samples (table 4). These cobalt dispersions, however, require that we reduce nitrate salts directly in hydrogen at very slow heating rates (< 12 K h^{-1}) without intermediate calcination steps [13–15]. Faster heating rates during reduction (240 K h^{-1}) gave lower dispersion eggshell catalysts (0.038). Calcination in air (673 K, 1 h) before reduction also decreased the Co dispersion (0.021).

Large, uniformly impregnated pellets (2.2 mm diameter) lead to lower cobalt–time yields, higher CH_4 selectivities, and lower activation energies (68 $\pm$ 8 kJ mol^{-1}) than Co/SiO_2 powders of much smaller diameter (115 $\pm$ 6 kJ mol^{-1}, 0.143 mm diameter) (table 4). FT synthesis rates, C_{5+} selectivities, and activation energies increase when large pellets are crushed and sieved to retain particles of smaller diameter (0.143 mm) (table 4). Clearly, reaction rates are inhibited by slow arrival of reactants within large pellets and the measured reaction rates are well

Table 4
Catalyst characterization and Fischer–Tropsch synthesis data on Co/SiO_2 (12.7–13.1% Co wt.) powders and even and eggshell large pellets (473 K, 2000 kPa, $H_2/CO = 2.1$, 55–65% CO conversion, >24 h on stream)

	Even large pellet	Crushed large pellet	Eggshell pellet	Crushed eggshell pellet	Small pellet
Co site density (10^6 (g-atom surface Co) m^{-2})	1.21	1.21	1.03 (3.6) [a]	1.03 (3.6) [a]	0.38
pellet size (mm)	2.2	0.17	2.2	0.17	0.17
silica surface area ($m^2\ g^{-1}$)	115	115	115	115	280
average pore diameter (nm)	32	32	32	32	13.5
impregnated pellet region (average eggshell thickness or pellet diameter) (mm)	2.2	0.17	0.23	0.17	0.17
characteristic diffusion length (mm)	1.1	0.085	0.23	0.085	0.085
Co dispersion (%)	6.3	6.3	5.5	5.5	5.0
structural parameter [b] ($m^{-1} \times 10^{-16}$)	21960	136	1908	272	95
site–time yield (h^{-1})	50	95	105	140	110
Co–time yield (h^{-1})	3.15	5.98	5.78	7.5	5.50
CH_4 selectivity (%)	12.1	5.2	7.7	4.7	7.0
C_{5+} selectivity (%)	81.5	89.6	88.0	90.5	83.5
CO_2 selectivity (%)	0.90	0.18	0.50	0.16	0.15
activation energy (kJ mol^{-1})	68	–	–	–	115

[a] Within impregnated shell region.
[b] $\chi = L^2\phi\theta/r_p$; r_p in m, site density (θ) in Co atoms/m^2, L as twice the characteristic diffusion distance (pellet radius or eggshell thickness) in m.

below intrinsic kinetic values. Similar improvements are obtained by placing Co sites within 0.1 mm of outer pellet surfaces. These eggshell catalysts are more active and selective for C_{5+} synthesis than uniformly impregnated large pellets. Cobalt–time yields and C_{5+} selectivity become even higher when these eggshell catalysts are crushed to form smaller pellets (table 4) because rates are influenced slightly by reactant diffusion even on these eggshell pellets. Reactant transport restrictions also influence methane selectivity and olefin content. The olefin content is higher on small or partially impregnated pellets, suggesting that low intrapellet CO concentrations within larger pellets increase secondary olefin hydrogenation rates. Large pellets also limit olefin removal rates and increase their intrapellet concentrations, additionally increasing hydrogenation and readsorption rates. Methane selectivity decreases as we eliminate transport restrictions, whether by partial impregnation or by decreasing pellet size, both of which decrease the distance that CO must travel to reach catalytic sites (table 4).

C_{5+} selectivities are actually higher on crushed eggshell catalysts than on Co/SiO_2 powders or crushed uniform pellets, even though FT synthesis pathways are not influenced by *reactant* transport restrictions on either sample. These selectivity differences reflect the higher local site densities on powders formed from egg-

shell samples, which are about four times greater than in crushed uniform samples and about 20 times greater than in Co/SiO_2 powders. As a result, the readsorption probability of reactive olefins, a reaction that initiates surface chains and increases product molecular weight and C_{5+} selectivity, is significantly greater on powders formed from eggshell pellets [1–4].

3.4. CATALYST STRUCTURE, INTRAPELLET SITE DISTRIBUTIONS, AND TRANSPORT RESTRICTIONS IN FT SYNTHESIS CATALYSTS

The effects of intrapellet Co distribution and site density reported here can be accurately described by a reaction–transport model described in detail elsewhere [3,4,15]. This model incorporates independent measurements of intrinsic kinetic parameters for CO hydrogenation steps with reported values of CO and H_2 diffusivities and solubilities within hydrocarbon liquids. The Thiele modulus (Φ) in this model is the product of two parameters

$$\Phi = \psi_{CO}\chi \cdot \tag{3}$$

The first term (ψ_{CO}) depends only on the reactive and diffusive properties of the diffusion-limited reactant (CO at our reaction conditions) [3,14,15]. The second term (χ) contains only structural catalyst parameters, such as the pellet radius or eggshell thickness (R_0), the areal density of active sites (θ) and the average SiO_2 support pore radius (r_p) of

$$\chi = \frac{R_0^2 \phi \theta_m}{r_p} \cdot \tag{4}$$

Higher χ values lead to more severe transport restrictions because the supply of reactants to catalytic sites becomes insufficient as R_0 and ϕ decrease and as higher consumption rates must be satisfied by transport for higher site densities (θ_m) or smaller pore radii (r_p).

Methane and C_{5+} selectivities obtained on Co supported on SiO_2, TiO_2, Al_2O_3 powders [16] and on Co/SiO_2 eggshell and uniform large impregnated pellets (table 4) are shown in fig. 3 as a function of the structural parameter χ. The C_{5+} selectivity initially increases as χ increases because reactant transport restrictions are negligible at low χ values but the readsorption of α-olefins, a reaction that increases product molecular weight, is enhanced by diffusion-limited intrapellet removal of these reactive molecules [1–5]. Methane selectivity decreases in the same range of χ values, also as a direct result of diffusion-enhanced α-olefin readsorption, because readsorbed α-olefins compete effectively for surface sites with C_1 initiators that readily form methane [1–4].

At higher χ values, C_{5+} selectivities reverse their initial increase because transport restrictions begin to influence reactant arrival and intrapellet CO concentrations. Methane selectivity also reverses its initial trend and increases as χ values increase. Similar trends are observed whether χ is varied by changing the character-

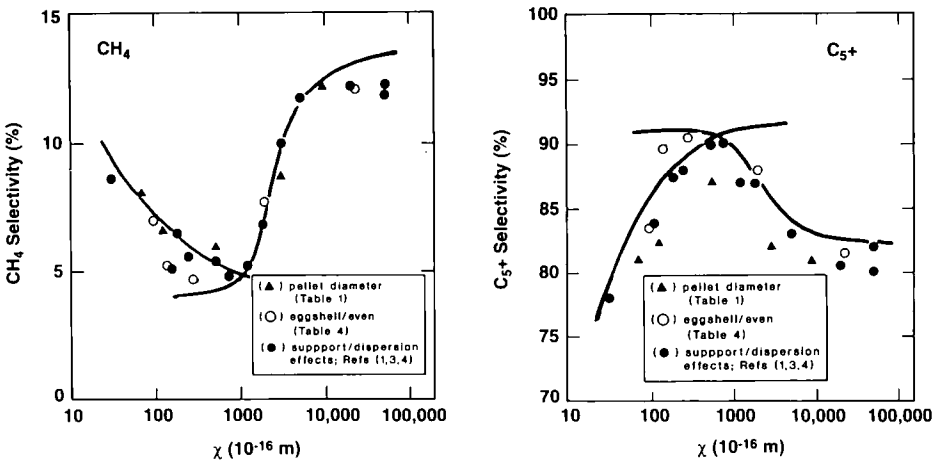

Fig. 3. The effect of structural catalyst parameters on the Fischer–Tropsch synthesis. (a) Methane selectivity, (b) C_{5+} selectivity. (Co on SiO_2, Al_2O_3, TiO_2, even and eggshell pellets; 473 K, 2000 kPa, $H_2/CO = 2.05$, 55–65% CO conversion).

istic diffusion distance (pellet diameter or eggshell thickness), the support porosity or pore radius, or the Co site density (fig. 3). These experimental results are accurately described by our reaction transport without any adjustable parameters (solid curves in fig. 3).

Pellets with intermediate χ values restrict olefin removal and enhance their readsorption but still permit rapid access of reactants to reaction sites and lead to highest C_{5+} selectivities. Our experimental data suggest that the design of optimum eggshell pellets requires materials with values of χ between 200 and 2000 $\times 10^{-16}$ m, which maximize C_{5+} selectivities and maintain FT synthesis rates near their intrinsic kinetic value. The eggshell syntheses techniques reported here allow the reproducible synthesis of catalyst pellets within this range of χ values, irrespective of the pellet size or site density required in the design of FT synthesis catalysts for use in packed-bed reactors.

Acknowledgement

We thank Dr. Rocco A. Fiato for many helpful discussions and Ms. Hilda Vroman and Mr. Bruce DeRites for the synthesis, characterization, and catalytic evaluation of some of the materials reported here. We also thank Dr. Eric Herbolzheimer and Ms. Dee Redd for the viscosity and surface tension measurements.

References

[1] E. Iglesia, S.L. Soled and R.A. Fiato, J. Catal. 137 (1992) 212.
[2] R.J. Madon, S.C. Reyes and E. Iglesia, J. Phys. Chem. 95 (1991) 7795.

[3] E. Iglesia, S.C. Reyes and S.L. Soled, in: *Computer-Aided Design of Catalysts and Reactors*, eds. E.R. Becker and C.J. Pereira (Dekker, New York, 1993) p. 199.
[4] E. Iglesia, S.C. Reyes, R.J. Madon and S.L. Soled, in: *Advances in Catalysis and Related Subjects*, Vol. 39, eds. D.D. Eley, H. Pines and P.B. Weisz (Academic Press, New York, 1993) p. 239.
[5] R.J. Madon, S.C. Reyes and E. Iglesia, in: *Selectivity in Catalysis*, ACS Symposium Series 517 eds. S.L. Suib and M.E. Davis (Am. Chem. Soc., Washington, 1992) p. 383.
[6] R.W. Maatman and C.D. Prater, Ind. Eng. Chem. 49 (1957) 253.
[7] W.E. Corbett and D. Luss, Chem. Eng. Sci. 29 (1974) 1473.
[8] C.J. Pereira, G. Kim and L.L. Hegedus, Catal. Rev. Sci. Eng. 26 (1984) 583; J.E. Summers and J.L. Hegedus, J. Catal. 51 (1978) 185.
[9] R.S. Dixit and L.L. Tavlarides, Chem. Eng. Sci. 37 (1982) 539; Ind. Eng. Chem. Proc. Des. Dev. 22 (1983) 1.
[10] R.C. Everson, E.T. Woodburn and A.R.M. Kirk, J. Catal. 53 (1978) 186.
[11] A. Neimark, A. Khelfez and V. Fenelonov, Ind. Eng. Chem. Prod. Res. Dev. 20 (1981) 439.
[12] M.F.M. Post and S.T. Sie, Eur. Patent Appl. 174,696 (1985); W.A. van Erp, J.M. Nanne and M.F.M. Post, US Patent 4,637,993 (1987).
[13] E. Iglesia, H. Vroman, S.L. Soled, J.E. Baumgartner and R.A. Fiato, US Patent 5,036,032 (1991); Eur. Patent Appl. 313,466 (1991); Eur. Patent Appl. 434,284 (1991).
[14] E. Iglesia, S.L. Soled and R.A. Fiato, US Patent 4,738,948 (1988); Eur. Patent Appl. 363,537 (1988).
[15] E. Iglesia, S.L. Soled, J.E. Baumgartner and S.C. Reyes, J. Catal., submitted.
[16] E. Iglesia, S.L. Soled and R.A. Fiato, J. Catal., in press.
[17] E. Washburn, Phys. Rev. 17 (1921) 273.